# ATLAS/ICESat-2 L3A Calibrated Backscatter Profiles and Atmospheric Layer Characteristics, Version 6

## USER GUIDE

**How to Cite These Data**

As a condition of using these data, you must include a citation:

Palm, S. P., Y. Yang, U. C. Herzfeld, D. W. Hancock III, K. A. Barbieri, J. Wimert, and the ICESat-2 Science Team. 2023. *ATLAS/ICESat-2 L3A Calibrated Backscatter Profiles and Atmospheric Layer Characteristics, Version 6*. [Indicate subset used]. Boulder, Colorado USA. NASA National Snow and Ice Data Center Distributed Active Archive Center. https://doi.org/10.5067/ATLAS/ATL09.006. [Date Accessed].

FOR QUESTIONS ABOUT THESE DATA, CONTACT NSIDC@NSIDC.ORG

FOR CURRENT INFORMATION, VISIT https://nsidc.org/data/ATL09

National Snow and Ice Data Center

# TABLE OF CONTENTS

# 1 DATA DESCRIPTION

## 1.1 Parameters

Calibrated, Attenuated Backscatter (CAB) profiles, layer-integrated attenuated backscatter, plus other parameters including cloud layer height and atmospheric characteristics.

## 1.2 File Information

### 1.2.1 Format

Data are provided as HDF5 formatted files.

### 1.2.2 ATLAS/ICESat-2 Description

NOTE: The following brief description of the Ice, Cloud and land Elevation Satellite-2 (ICESat-2) observatory and Advanced Topographic Laser Altimeter System (ATLAS) instrument is provided to help users better understand the file naming conventions, internal structure of data files, and other details referenced by this user guide. The ATL09 data product is described in detail in the ICESat-2 Algorithm Theoretical Basis Document for the Atmosphere, Part I: Level 2 and 3 Data Products (ATL04/09 ATBD Part I V6 | https://doi.org/10.5067/H975R4YYVIT6) and Part II: Level 2 and 3 Data Products (ATL04/09 ATBD Part II V6 | https://doi.org/10.5067/CP08GNGYS4YJ). Only ATL04/09 ATBD Part I is referenced in this user guide.

The ICESat-2 observatory utilizes a photon-counting lidar (the ATLAS instrument) and ancillary systems (GPS, star cameras, and ground processing) to measure the time a photon takes to travel from ATLAS to Earth and back again and determine the reflected photon's geodetic latitude and longitude. Laser pulses from ATLAS illuminate three left/right pairs of spots on the surface that trace out six approximately 14 m wide ground tracks as ICESat-2 orbits Earth. Each ground track is numbered according to the laser spot number that generates it, with Ground Track 1L (GT1L) on the far left and Ground Track 3R (GT3R) on the far right. Left/right spots within each pair are approximately 90 m apart in the across-track direction and 2.5 km in the along-track direction The ATL09 data product is organized by ground track, with ground tracks 1L and 1R forming pair one, ground tracks 2L and 2R forming pair two, and ground tracks 3L and 3R forming pair three. Each pair also has a Pair Track—an imaginary line halfway between the actual location of the left and right beams (see Figure 1). Pair tracks are approximately 3 km apart in the across-track direction.

The beams within each pair have different transmit energies—so-called weak and strong beams—with an energy ratio between them of approximately 1:4. The mapping between the strong and weak beams of ATLAS, and their relative position on the ground, depends on the orientation (yaw) of the ICESat-2 observatory, which is changed approximately twice per year to maximize solar

illumination of the solar panels. The forward orientation corresponds to ATLAS traveling along the +x coordinate in the ATLAS instrument reference frame (see Figure , left). In this orientation, the weak beams lead the strong beams and a weak beam is on the left edge of the beam pattern. In the backward orientation, ATLAS travels along the -x coordinate, in the instrument reference frame, with the strong beams leading the weak beams and a strong beam on the left edge of the beam pattern (see **Error! Reference source not found.**). The first yaw flip was performed on 28 December 2018, placing the spacecraft into the backward orientation. ATL09 reports the spacecraft orientation in the `sc_orient` parameter stored in the `/orbit_info/` data group (see Section 1.2.4 Data Groups). The current spacecraft orientation, as well as a history of previous yaw flips, is available in the ICESat-2 Major Activities tracking document (`.xlsx`).

The Reference Ground Track (RGT) refers to the imaginary track on Earth at which a specified unit vector within the observatory is pointed. During nominal operating conditions onboard software aims the laser beams so that the RGT is between ground tracks 2L and 2R (i.e., coincident with Pair Track 2). The ICESat-2 mission acquires data along 1,387 different RGTs. Each RGT is targeted in the polar regions once every 91 days to allow elevation changes to be detected. Cycle numbers track the number of 91-day periods that have elapsed since the ICESat-2 observatory entered the science orbit. RGTs are uniquely identified, for example in ATL02 file names, by appending the two-digit cycle number (cc) to the RGT number, e.g., 0001cc to 1387cc.

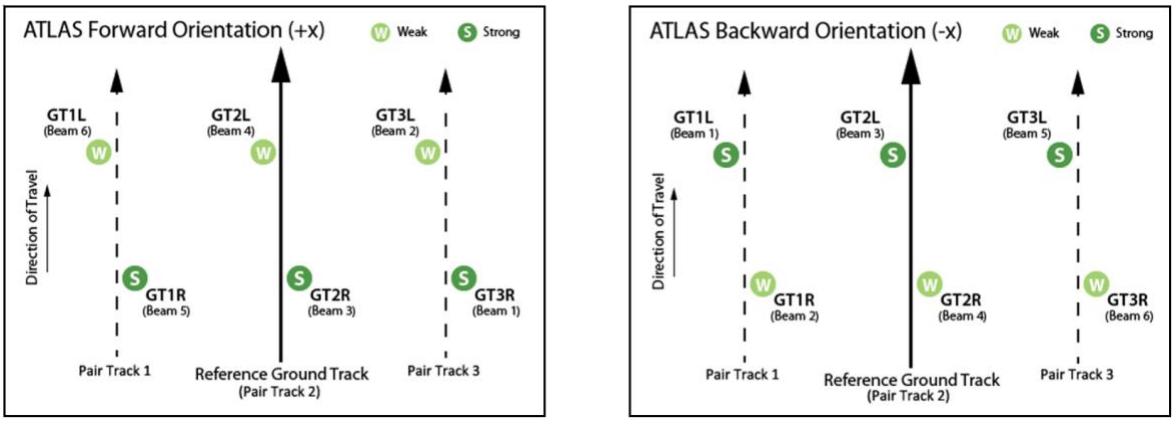


Figure 1. Spot and ground track (GT) naming convention with ATLAS oriented in the forward (instrument coordinate +x) direction and backward (instrument coordinate -x) direction.

Under normal operating conditions, data are not collected along the RGT; however, during spacecraft slews, or off-pointing, some ground tracks may intersect the RGT. Off-pointing refers to a series of plans over the mid-latitudes that have been designed to facilitate a global ground and canopy height data product with approximately 2 km track spacing. Off-pointing began on 1 August 2019 with RGT 518, after the ATLAS/ICESat-2 PPD and POD solutions had been adequately

resolved and the instrument had pointed directly at the reference ground track for at least a full 91 days (1,387 orbits).

Users should note that sometimes, for various reasons, the spacecraft pointing may lead to ICESat-2 data collected offset at some distance from the RGTs instead of along the nominal RGT. Although not along the nominal RGT, the geolocation information and data quality for these data are not degraded. As an example, from 14 October 2018 and 30 March 2019, the spacecraft pointing control was not yet optimized. To identify such time periods, refer to the ICESat-2 Major Activities file.

NOTE: ICESat-2 reference ground tracks with dates and times can be downloaded as KMZ files from NASA's ICESat-2 | Technical Specs page, below the Orbit and Coverage table.

Unlike ATLAS-derived altimetry, which utilizes both weak and strong beams, atmospheric profiles are generated from strong beams only: beams 1, 3, and 5. The ATL09 product contains three corresponding atmospheric profiles numbered 1, 2, and 3 from left to right, relative to the direction of spacecraft travel. Note, however, that the instrument orientation determines which beam corresponds to which profile. With ATLAS in the forward spacecraft orientation (+x), beam 1 lies to the left of the nadir ground track (profile 1), beam 3 lies along the nadir track (profile 2), and beam 5 is to the right (profile 3). The backward orientation reverses the locations on the ground of beams 1 and 5 (beam 3 remains in the center regardless of orientation), with beam 5 to the left of nadir (profile 1) and beam 1 (profile 3) to the right.

Various reference systems and dynamic processes, or geophysical corrections, occur during an ATLAS/ICESat-2 measurement (Figure 2). Table 1 lists the corrections needed for each surface type and ICESat-2 product. For example, to determine an estimate of the mean sea surface, several well-modeled, time-varying effects must be accounted for.

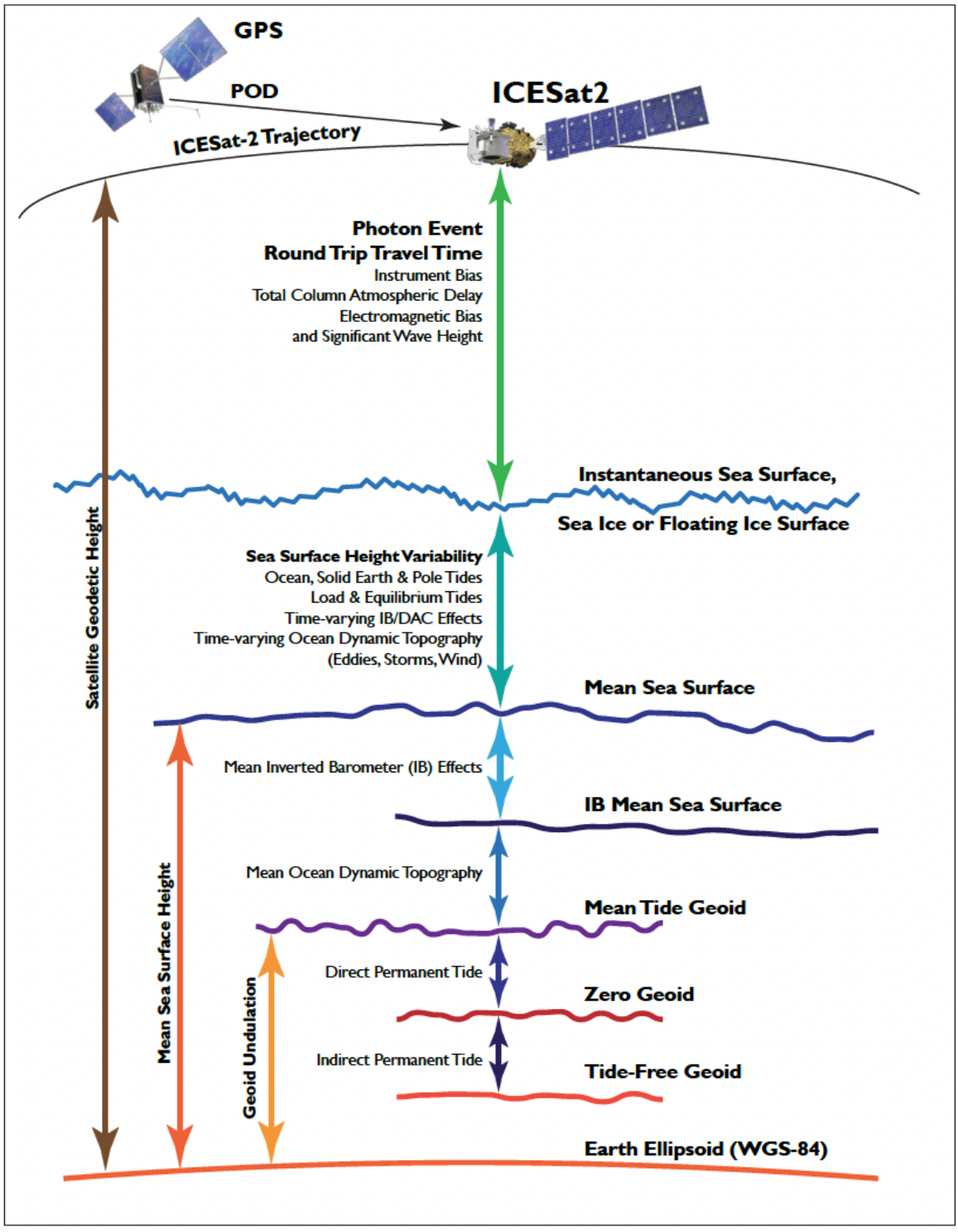


Figure 2. Geophysical corrections used in satellite altimetry. Taken from *ICESat-2 Data Comparison User's Guide for Rel006* available on the ATL03 data set landing page.

Table 1. Geophysical Corrections Applied to ICESat-2 Products

| ICESat-2 Products by Surface Type | Geophysical Corrections[1] |
|---|---|
| Photon-level product (ATL03) (i.e., corrections applicable across all surface types) | Ocean loading<br>Solid Earth tide<br>Solid Earth pole tide<br>Ocean pole tide<br>Total column atmospheric range-delay |
| Land Ice, Land, and Inland Water (ATL06, ATL08, and ATL13) | *No corrections beyond ATL03* |
| Sea Ice (ATL07 and ATL10) | Referenced to mean sea surface<br>Ocean tide<br>Long period equilibrium ocean tide<br>Inverted barometer (IB) |
| Ocean (ATL12) | Ocean tide<br>Long period equilibrium ocean tide |

[1]For details, see Section 5 of the *ICESat-2 Data Comparison User's Guide for Rel006* available on the ATL03 data set landing page.

### 1.2.3 File Naming Convention

ATL09 data are provided as granules (files) that span one orbit (i.e., one RGT). Data files utilize the following naming convention:

```
ATL09_[yyyymmdd][hhmmss]_[ttttccss]_[vvv_rr].h5
```

Example:

```
ATL09_20181014000347_02350101_006_01.h5
```

The following table describes the file naming convention variables:

Table 2. File Naming Convention Variables and Descriptions

| Variable | Description |
|---|---|
| `ATL09` | ATLAS/ICESat-2 L3A Calibrated Backscatter Profiles and Atmospheric Layer Characteristics data product |
| `yyyymmdd` | Year, month, and day of data acquisition |
| `hhmmss` | Hour, minute, and second of data acquisition (UTC) |
| `RGT` | Reference Ground Track. The ICESat-2 mission has 1,387 RGTs, numbered from 0001 to 1387. |
| `cc` | Cycle Number. Each of the 1387 RGTs is targeted in the polar regions once every 91 days. The cycle number tracks the number of 91-day periods that have elapsed since ICESat-2 entered the science orbit. |

| Variable | Description |
|---|---|
| ss | Segment number, always "01" for ATL04/09.[1] |
| vvv_rr | Version and revision number.[2] |

[1] Some ATLAS/ICESat-2 products (e.g., ATL03) are provided as files that span 1/14th of an orbit. As such, these products' file names specify a segment number that ranges from 01 to 14. Because ATL04 and ATL09 data files span one full orbit, the segment number is always set to 01.

[2] From time to time, NSIDC receives reprocessed granules from our data provider. These granules have the same file name as the original (i.e., date, time, ground track, cycle, and segment number), but the revision number has been incremented. Although NSIDC deletes the superseded granule, the process can take several days. If you encounter multiple granules with the same file name, please use the granule with the highest revision number.

Each data file has a corresponding XML file that contains additional science metadata. XML metadata files have the same name as their corresponding .h5 file, but with .xml appended.

### 1.2.4 Data Groups

Within data files, similar variables such as science data, instrument parameters, orbit information, and metadata are grouped together according to the HDF model. ATL09 data files contain the top-level groups shown in the following figure:

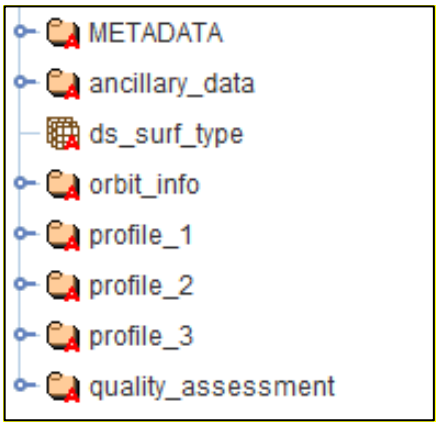


Figure 1. Top-level data groups displayed in HDFView.

The following sections summarize the structure and primary variables of interest in ATL09 data files. Additional details are available in "Section 4.2 | L3 Outputs" of the ATL04/09 ATBD Part I. For a complete list of all ATL09 parameters, see the ATL09 Data Dictionary.

#### 1.2.4.1 METADATA

ISO19115 structured summary metadata.

#### 1.2.4.2 ancillary_data

Ancillary information such as product and instrument characteristics and processing constants.

#### 1.2.4.3 orbit_info

Parameters that are constant for a granule, such as the RGT number, cycle number, and spacecraft orientation (`sc_orient`).

#### 1.2.4.4 profile_[x]

The `profile_1`, `profile_2`, and `profile_3` data groups each contain three subgroups:

**`/bckgrd_atlas/`**
ATLAS 50-shot background data and derivations from ATL03 used to determine the background for method 3 (see ATL03 ATBD Section 7.3 and ATL04/09 ATBD Part I Section 3.3.4)

**`/high_rate/`**
Parameters related to CAB at 25 Hz, including CAB profiles (`cab_prof`) from -1 to 20 km for the leftmost, center, and rightmost groundtracks with respect to the satellite direction of motion; latitudes and longitudes; parameters related to the background calculation; blowing snow layer characteristics; cloud characteristics; atmospheric layer characteristics; and high-, medium-, and low-confidence signal photon counts and statistics.

**`/low_rate/`**
Parameters related to atmospheric characteristics at 1 Hz, including blowing snow layer characteristics and atmospheric layer characteristics (pressure, specific humidity, temperature, total column liquid water and cloud ice, and component winds).

#### 1.2.4.5 quality assessment

Quality assessment data for the granule overall, plus summary QA data. QA parameters include statistical metrics for each profile related to: CAB and Apparent Surface Reflectance; cloud detection results; cloud optical depth (COD); surface detection; and ocean surface reflectance.

#### 1.2.4.6 ds_surf_type

This parameter, stored at the top level alongside the data groups, is a dimension scale variable indexing the surface type array (`/profile_[x]/surf_type`).

### 1.2.5 Browse Files

Browse files are provided as JPGs containing images designed to quickly assess the location and quality of each granule's data.

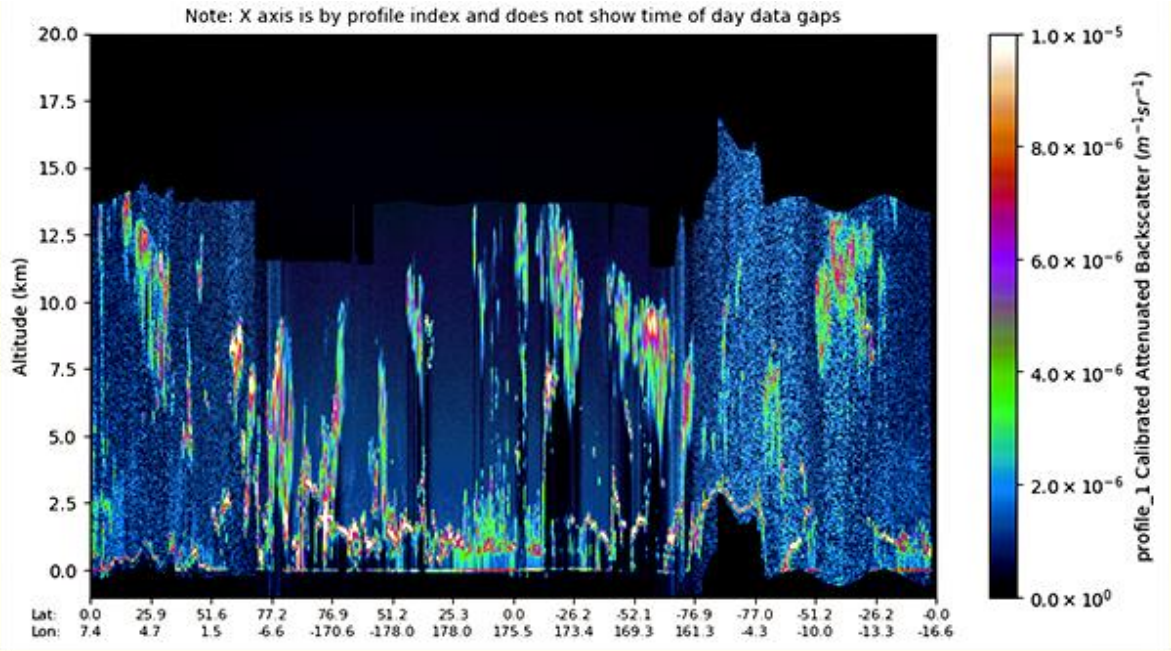


Figure 2. Sample browse image (`cab_profile`) showing CAB.

Browse files utilize the same naming convention as their corresponding data file but with "`_BRW`" and descriptive keywords appended.

## 1.3 Spatial Information

### 1.3.1 Coverage

The ICESat-2 mission acquires data along 1,387 reference ground tracks.

### 1.3.2 Resolution

The atmospheric profiles consist of 30 m bins in a 14 km tall column, where the top is nominally 13.75 km above and the bottom is -0.25 km below the local value of the digital elevation model (DEM) (see "pulse aliasing" in Section 1 of the ATL04/09 ATBD). After summing 400 shots, the three strong beams are downlinked to produce three 25 Hz profiles with a 280 m along-track resolution.

### 1.3.3 Geolocation

The following table provides information this data set's coordinate system.

Table 3. Geolocation Details

| | |
|---|---|
| Geographic coordinate system | WGS 84 |
| Projected coordinate system | WGS 84 |
| Longitude of true origin | Prime Meridian, Greenwich |
| Latitude of true origin | N/A |
| Scale factor at longitude of true origin | N/A |
| Datum | WGS 84 |
| Ellipsoid/spheroid | WGS 84 |
| Units | degree |
| False easting | N/A |
| False northing | N/A |
| EPSG code | 4326 |
| PROJ4 string | +proj=longlat +datum=WGS84 +no_defs |
| Reference | https://epsg.io/4326 |

## 1.4 Temporal Information

### 1.4.1 Coverage

14 October 2018 to present

### 1.4.2 Resolution

Each of ICESat-2's 1387 RGTs is targeted in the polar regions once every 91 days (i.e., the satellite has a 91-day repeat cycle).

Note that satellite maneuvers, data downlink issues, and other events can introduce data gaps into the ICESat-2 suite of products. ATL03 acts as the bridge between the lower level, instrumentation-specific data and the higher-level products. On the data set landing page, users can download and consult a regularly updated list of ATL03 data gaps (.xlsx).

# 2 DATA ACQUISITION AND PROCESSING

## 2.1 Background

ATL09 consists of CAB profiles, plus other parameters including layer integrated attenuated backscatter, cloud layer height, and numerous atmospheric characteristics obtained from the data.

CAB is generated from the Normalized Relative Backscatter (NRB) profiles and calibration constant computed in the ATL04 product. The following figure shows the ATLAS/ICESat-2 data processing flow.

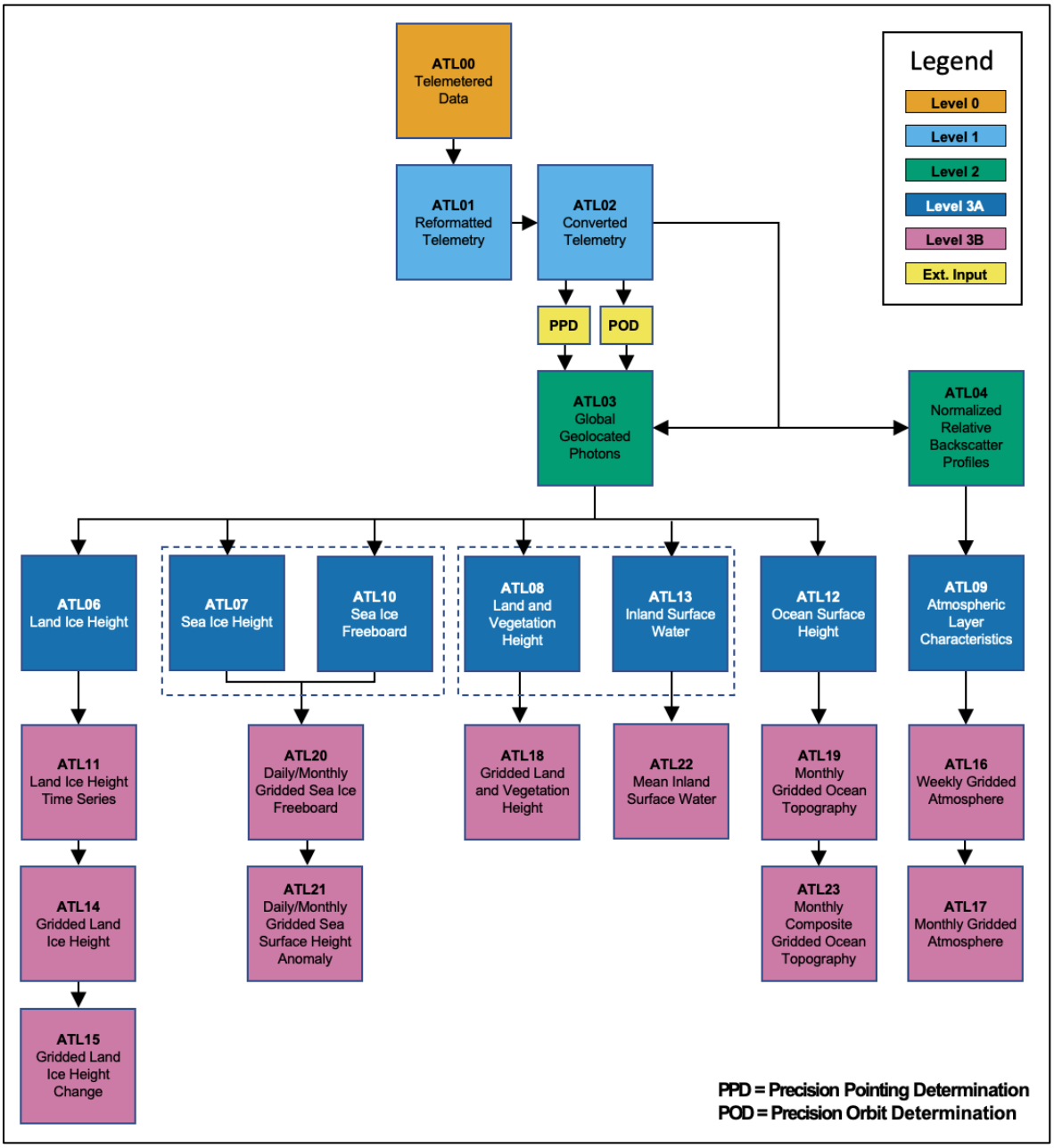


Figure 3. Schematic of the ICESat-2 data processing flow. The ATL01 algorithm reformats and unpacks the Level-0 data and converts it into engineering units. ATL02 processing converts ATL01 data to science units and applies instrument corrections. The Precision Pointing Determination (PPD) and Precision Orbit Determination (POD) solutions compute the pointing vector and position of the ICESat-2 observatory as a function of time.

## 2.2 Acquisition

To acquire high resolution altimetry measurements, ATLAS uses a high repetition rate laser (10 KHz). Each laser pulse is separated by only 30 km in the vertical. Thus, when a pulse (pulse 1) strikes the ground, the laser pulse right after it (pulse 2) is at 30 km altitude. When the ground return from pulse 1 reaches 15 km altitude (on its way back to the satellite), laser pulse 2 is at 15 km also (but travelling downward). The atmospheric return from pulse 2 (from 15 km altitude) travels back to the receiver at the same time as the ground return from pulse 1.

The atmospheric scattering that is recorded by the instrument at height H (km) is the sum of the scattering at height H, H+15, H-15, H+30, H-30, H+45, H-45, etc.

### 2.2.1 Inputs

The following inputs are used to generate the ATL09 product:

- The current ATL04 granule, plus the preceding and subsequent granules;
- NOAA Global Multi-sensor Snow/Ice Cover Map;
- Surface albedo (produced by the ICESat-2 Science Team; see Section 4.6.2, ATL04/09 ATBD Part I).

Algorithm adjustable parameters that are read in and used by the ATL09 algorithm are listed in Table 4.2 of the ATL04/09 ATBD Part I.

### 2.2.2 Outputs

ATL09 contains numerous parameters related to CAB, blowing snow, and atmospheric characteristics. Output parameters are listed in Table 4.1 of the ATL04/09 ATBD Part I. The following list contains the location of some of the key ATL09 output parameters. References to ATL04 denote values that are input from the ATL04 product. All other values are computed within ATL09:

- **`profile_[x]/high_rate/` (25 Hz)**
  - `backg_c` — background (ATL04)
  - `backg_theoret` — theoretical background
  - `bsnow_con` — blowing snow confidence
  - `bsnow_h` — height, blowing snow layer top
  - `bsnow_od` — optical depth, blowing snow layer
  - `cab_prof` — calibrated attenuated backscatter profile
  - `cap_h` — height, clear air precipitation top
  - `cloud_flag_asr` — cloud probability from apparent surface reflectance
  - `cloud_flag_atm` — number of cloud/aerosol layers detected computed
  - `column_od_asr` — optical depth of atmosphere column from apparent surface reflectance

    - `layer_attr` — layer type flag, where 1 = cloud, 2 = aerosol, 3 = unknown, 4 = blowing snow, 5 = blowing snow and diamond dust, 6 = diamond dust (wind speed > `bs_thresh_wind`), 7 = diamond dust (wind speed ≤ `bs_thresh_wind`)
    - `layer_bot` — height, bottom of detected layers
    - `layer_con` — layer confidence flag
    - `layer_ib` — layer integrated backscatter
    - `layer_top` — height, top of detected layers
    - `ocean_surf_reflec` — ocean surface reflectance
- **`profile_[x]/low_rate/` (1 Hz)**
    - `bsnow_con` — blowing snow confidence (see Table 4 below)
    - `bsnow_h` — height, blowing snow layer top
    - `bsnow_od` — optical depth, blowing snow layer
    - `cal_c` — calibration coefficient for each beam
    - `cap_h` — height, clear air precipitation top
    - `mol_backscatter` — molecular backscatter profile (ATL04)
- **`ancillary_data/atmosphere/` (1 per granule)**
    - `backg_select` — method used to calculate background (ATL04)
    - `cal_select` — the calibration method used in the NRB calculation (ATL04)

## 2.3 Processing

### 2.3.1 Calibrated Attenuated Backscatter

The following section briefly describes the approach used to compute CAB from NRB. For a complete description, see Section 3.3 of the ATL04/09 ATBD Part I.

CAB profiles are computed by simply dividing NRB profiles by a calibration coefficient that is computed in ATL04 and passed to ATL09. To compute NRB, three corrections are applied to the raw level 0 data: laser energy normalization, range square correction, and background subtraction. The lidar equation is

$$S(z) = \frac{CE\beta(z)T^2(z)}{r^2} + p_b + p_d$$

In the equation above, S(z) is the measured raw signal (photons) at height z; r is the range from the spacecraft to the height z; C is the lidar system calibration coefficient; E is the laser energy; β(z) is the 180° backscatter coefficient at height z; T(z) is the one-way atmospheric transmission from the spacecraft to height z; $p_b$ is the solar background; and $p_d$ is the detector dark count rate.

NRB is generated for each of the strong beams using

$$NRB(z) = \frac{(S(z) - p_b - p_d)r^2}{E}$$

CAB is then computed by dividing the NRB by the calibration coefficient C:

$$\beta(z)T(z)^2 = \frac{NRB(z)}{C}$$

The calibration coefficient is computed only over the polar regions, typically 3 - 4 values per orbit. To ensure the calibration values used in ATL09 have a smooth transition from granule to granule, the algorithm uses the last calibration point from the prior ATL04 granule, all calibration points from the current ATL04 granule, and the first calibration point from the next granule. Calibration values at any time t within a granule are computed using a linear, piece-wise interpolation between calibration points. "Section 4.3 | Calibrated, Attenuated Backscatter Profiles" in the ATL04/09 ATBD Part I for describes alternate interpolation strategies used if calibration values are not available for the prior or subsequent ATL04 granules.

### 2.3.2 Apparent Surface Reflectance

The Apparent Surface Reflectance (ASR) is essentially the received laser pulse energy from the surface divided by the transmitted laser pulse energy, multiplied by the two-way atmospheric transmission ($T^2$). For example, in the case of a planetary body with no atmosphere, like the moon, the ASR would equal the actual surface reflectance at the laser wavelength. On Earth however, the ASR is modified by the atmospheric transmission, which in general is not known. For a clear atmosphere, $T^2$ is about 0.81 at sea level (at 532 nm). Clouds and aerosols introduce further transmission loss ranging from a few tenths to a few orders of magnitude. This means that the ASR will always be less than the actual surface reflectance. For example, if snow has a reflectance of 0.9 at 532 nm, then the ASR measured through a clear atmosphere at sea level will be 0.73 (0.81 x 0.9). If the surface reflectance is known well enough, the ratio of the apparent surface reflectance to the actual surface reflectance can be used as a relative measure of $T^2$ and thus as an indicator of the likely presence of clouds. The ASR calculation for ATLAS/ICESat-2 is detailed in "Section 4.7 | Apparent Surface Reflectance (ASR)" of the ATL04/09 ATBD Part I.

### 2.3.3 Cloud Detection

Clouds lower the returning energy that is reflected by the surface and thus lower the ASR. When clouds are present, the ASR is a function of COD, but also to a lesser degree, cloud height and cloud microphysical properties. For example, based on model simulations, a cloud with a COD = 0.1 decreases the surface return by about 8% to 17%; a cloud with a COD = 1.0 decreases the surface return by 57% to 85%. As such, the cloud signal in ASR is strong enough to be used for cloud detection. Given that clouds can significantly reduce the ASR measured by ATLAS detectors, it is possible to set a threshold to differentiate cloudy from clear conditions. The ASR cloud detection method and implementation are described in detail in "Section 4.7.1 | Cloud Detection

using ASR" and "Section 4.7.2 | ASR Cloud Detection Algorithm Implementation" of the ATL04/09 ATBD Part I.

## 2.4 Quality, Errors, and Limitations

Because of the various limitations of the ICESat-2 atmospheric data, and the likelihood that only a few calibration points will be obtained per orbit, the calibration error and confidence are difficult to establish. The Science Team is evaluating methods to mitigate and more rigorously quantify calibration error on an ongoing basis.

The browse file corresponding to each data granule contains a number of plots and images that can be used to assess the quality of ATL09 data. See Section 6.0 | Quality Assessment in the ATL04/09 ATBD Part I for brief descriptions. In addition, QA parameters for each profile are stored in the top-level `quality_assesment/` data group, including statistical metrics that describe CAB and ASR, cloud detection results, COD, surface detection, and ocean surface reflectance.

Potential sources and magnitudes of error in the ATL04 NRB computation, which is passed to ATL08, are discussed in Section 3 of the ATL04/09 ATBD Part I, particularly Sections 3.3.2.1 | Error Analysis of Molecular Contribution and 3.3.7.4 | Calibration Error and Confidence. Errors and uncertainties in input sources to ATL04, including ATL02 and ATL03, can propagate into downstream products. Users interested in these error sources should consult the ATBDs for ATL02 and ATL03.

# 3 VERSION HISTORY

A summary of the version history is provided in Table 4, followed by a detailed list of changes for the current version.

Table 4. Version History Summary

| Version | Release Date | Description |
|---|---|---|
| V1 | May 2019 | Initial release |
| V2 | October 2019 | Refer to V2 User Guide |
| V3 | May 2020 | Refer to V3 User Guide |
| V4 | April 2021 | Refer to V4 User Guide |
| V5 | November 2021 | Refer to V5 User Guide |
| V6 | May 2023 | • Modified blowing snow detection algorithm to reduce false positive detections often seen in daylight.<br>• Added and modified the blowing snow confidence values (`bsnow_con`) to include new descriptions and changed the parameter from a one-byte to a two-byte integer value. See Table 4. |

| | | |
|---|---|---|
| | | • Added four values to the layer attribute parameter (`layer_attr`). See Section 2.2.2.<br>• Added a new parameter called clear air precipitation top height (`cap_h`) that denotes the top height of clear air precipitation that reached the ground.<br>• Replaced the ANC32 surface reflectance map (now based on three years of ICESat-2 surface reflectance measurements instead of two) to fill in gaps.<br>• Changed `bs_quartile` to `bs_quantile` in ATL09 and related code.<br>• Modified code to use density matrix 1 instead of density matrix 2 when computing layer densities.<br>• Implemented a third pass of the density dimension algorithm to reduce the effect of noise in creating false layers.<br>• Updated the ANC45 cloud/aerosol discrimination table to increase the accuracy of detected layers. |
| V6.1 | May 2024 | Data from 13 November 2022 to 26 October 2023 were reprocessed using ITRF2014 (replacing ITRF2020) for consistency across the entire data set. |

# 4 REFERENCES

Bodhaine B. A., Wood, N. B., Dutton, E. G., & Slusser, J. R. (1999). On Rayleigh optical depth calculations. *Journal of Atmospheric and Oceanic Technology, 16*, 1854–1861. https://doi.org/10.1175/1520-0426(1999)016<1854:ORODC>2.0.CO;2

Essery, R., Long, L., & Pomeroy, J. (1999). A distributed model of blowing snow over complex terrain. *Hydrological Processes, 13*, 2423–2438. https://doi.org/10.1002/(SICI)1099-1085(199910)13:14/15<2423::AID-HYP853>3.0.CO;2-U

Iqbal, M. (1983). *An Introduction to Solar Radiation.* Academic Press.

Ismail, S., & Browell, E. (1989). Airborne and spaceborne lidar measurements of water vapor profiles: a sensitivity analysis. *Applied Optics, 28*, 3603–3615. https://doi.org/10.1364/AO.28.003603

Lambert, A., Bailey, P. L., Edwards, D. P., Gille, J. C., Halvorson, C. M., Johnson, B. R., Massie, S. T., & Stone, K. A. (1999). High Resolution Dynamics Limb Sounder Level-2 Algorithm Theoretical Basis Document. https://eospso.gsfc.nasa.gov/sites/default/files/atbd/ATBD-HIR-02.pdf

She, C.-Y. (2001). Spectral structure of laser light scattering revisited: Bandwidths of nonresonant scattering lidars. *Applied Optics, 40*(27), 4875–4884. https://doi.org/10.1364/AO.40.004875

Vigroux, E. (1953). Contribution a l'etude experimentale de l'absorption de l'ozone. *Annales de Physique, 8*, 709–761. https://doi.org/10.1051/anphys/195312080709

# 5 DOCUMENT INFORMATION

## 5.1 Publication Date

May 2023

## 5.2 Date Last Updated

May 2024